Effective Morphology Control in an Immiscible Crystalline/Crystalline Blend by Artificially Selected Viscoelastic Phase Separation Pathways

ARTICLE *in* MACROMOLECULES · FEBRUARY 2014

Impact Factor: 5.8 · DOI: 10.1021/ma5001496

6 AUTHORS, INCLUDING:

Fenghua Chen
Chinese Academy of Sciences
17 PUBLICATIONS **192** CITATIONS
SEE PROFILE

Wei Liu
Peking University
576 PUBLICATIONS **7,625** CITATIONS
SEE PROFILE

Yongri Liang
Beijing Institute of Petrochemical Technology
46 PUBLICATIONS **408** CITATIONS
SEE PROFILE

Macromolecules

Article

pubs.acs.org/Macromolecules

Effective Morphology Control in an Immiscible Crystalline/Crystalline Blend by Artificially Selected Viscoelastic Phase Separation Pathways

Zhiyuan He,[†,‡] Weichao Shi,[†] Fenghua Chen,[†] Wei Liu,[†] Yongri Liang,*[,†,§] and Charles C. Han*[,†]

[†]State Key Laboratory of Polymer Physics and Chemistry, Joint Laboratory of Polymer Science and Materials, Beijing National Laboratory for Molecular Sciences, Institute of Chemistry, Chinese Academy of Sciences, Beijing 100190, P. R. China

[‡]University of Chinese Academy of Sciences, Beijing 100049, P. R. China

[§]College of Materials Science and Engineering, Beijing Institute of Petrochemical Technology, Beijing 102617, P. R. China

Supporting Information

ABSTRACT: We investigated the interplay between viscoelastic phase separation (VPS) and crystallization in a dynamically asymmetric crystalline/crystalline polymer blend system of poly(butylene succinate) (PBS)/poly(ethylene oxide) (PEO). The dynamic asymmetry came from the large molecular weight difference between the slow relaxing PEO and the fast relaxing PBS molecules. The evolution of network-like structures, phase inversion, and volume shrinking processes were studied by a phase contrast microscope (PCOM). The crystallization kinetics of PBS was determined by a differential scanning calorimeter (DSC). It was found that both the crystal nucleation and growth of PBS were strongly influenced by the existence and relaxation of the entangled PEO network, even though PEO was the minor component. The nuclei of PBS were more inclined to form at the interface between phase domains due to the effect of interface-assisted crystallization. Thus, the nucleation density decreased with the decrease of interfacial area. Meanwhile, the corresponding crystal growth rate was also dependent on the VPS processes. After a second quench to a temperature below the melting point of PEO, the spatial distribution of both components and the final crystallization morphology were also significantly controlled by the initial phase structures. Compared to dynamically symmetric polymer systems, the VPS process provided more versatile pathways to control the phase and crystallization morphologies in such immiscible crystalline/crystalline polymer blends.

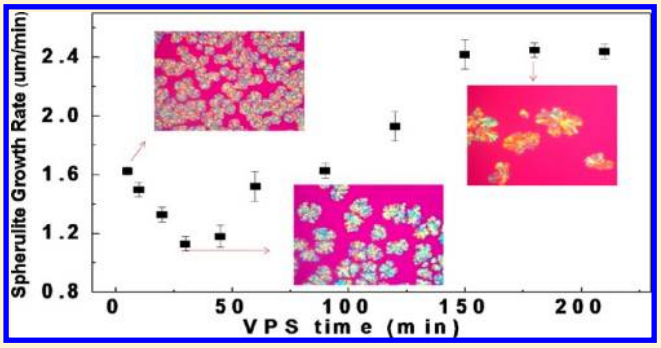

1. INTRODUCTION

Considerable attention has been paid to phase morphology control in polymer blends in order to meet the functional needs through manufacturing processes.[1−3] Owing to the negligible mixing entropy, most binary polymer mixtures are thermodynamically immiscible. In the blend systems with dynamic symmetry, the typical "bicontinuous" and "sea−island" phase structures can be selectively controlled by spinodal decomposition.[4,5] However, for most of the immiscible blends, the minor component always disperses as droplets in the matrix of the majority one, leading to a few features and properties.[6,7]Recently, it has been reported that a large number of novel phase morphologies can be produced by employing the dynamically asymmetric phase separation or viscoelastic phase separation (VPS).[8−10] Compared with the normal phase separation, the dynamic asymmetry for a binary blend is mainly enhanced by the large difference between molecular weights and/or glass transition temperatures of the two components.[11−13] As the slow component relaxes much slower than the concentration growth, then it induces an internal network stress. As a result, the slow component, even if the content is extremely low, is able to form the interconnected phase domains and network-like structures.[14−16] So the VPS process will offer a powerful tool for adjusting the structure and property of polymer blends.

Crystallization[17−19] and phase separation are important phase transitions which have been widely studied theoretically and experimentally. When phase separation and crystallization occur simultaneously, the final morphology and property of the polymer blends are controlled by the pathways determined by the competition and interaction between these phase transitions.[20−24] Recently, Han and co-workers have carried out a series of experiments on the interplay between liquid−liquid phase separation (LLPS) and crystallization in the dynamically symmetric blends of polyolefin with upper critical solution temperature (UCST) type of phase diagram.[25−27] It is reported that the concentration fluctuation caused by the spinodal decomposition can assist the primary nucleation of crystallization, especially at the interface of phase domains. During the interdiffusion process of spinodal decomposition, the moving polymer chains can induce local segment alignment or orientation, which may help overcome the usual nucleation

Received: January 20, 2014
Revised: February 21, 2014
Published: February 27, 2014

   dx.doi.org/10.1021/ma5001496 | Macromolecules 2014, 47, 1741−1748

energy barrier. On the other hand, according to the simulation results of Mitra and Muthukumar, the formation of phase domains provide interfaces for heterogeneous nucleation, which can help decreasing the surface energy of crystallizing embryos and assisting the crystallization.[28] Actually, the contributions of these two factors should coexist and can hardly be distinguished and quantified separately when both mechanisms of nucleation occur simultaneously. Up to now, despite that much progress on phase transitions has been achieved, the issues of multiple simultaneous phase transitions still remain as a challenge. The physics of such phenomena is complicated, which involves the crossover effect of dynamics and thermodynamics. However, it is difficult to obtain more new and convincing data in dynamically symmetric systems to help us understand further the coupled phase transitions due to the fast and coupled dynamics of the two components involved. On the contrary, there were many advantages of employing dynamically asymmetrical systems: the dynamics of both viscoelastic phase separation and crystallization could be more differentiable and controllable; the interfaces of phase domains were sharp and clear; the phase domains could not be easily distorted by hydrodynamic interaction and many direct evidence could be obtained just by microscopy on a large dimensional scale.[16]

Up to now, only a few studies have been reported on the dynamic competition between phase separation and crystallization in the dynamically asymmetric systems.[29−31] Shi and co-workers have studied the frustrated crystallization coupled with a simultaneous VPS process in a dynamically asymmetric blend of PMMA/PEO. They proposed that the network stress in the concentration growth led to the frustration of crystallization.[29] Shi have also investigated a variety of novel crystalline pattern formations via mediating the dynamics between VPS process and crystallization.[30,31] Recently, the effect of VPS process on the interface assisted crystallization has been studied in a highly immiscible iPP/PMMA blend. It is reported that the final property of blend could be controlled between the properties of neat iPP and PMMA when the PMMA phase inverted from the transient network to dispersed domains.[16] Although some progress has been achieved until present, many essential problems still have not been solved: How do the crystals nucleate under the effect of pre-existed phase morphologies when these dual phase transitions occur separately (in a LCST system)? How do the crystals grow under the effect of network stress? How can the final crystallization morphology be controlled via the control of initial phase structures when both components are able to crystallize.

Recently, compared with amorphous/crystalline polymer blend systems, many studies have concerned on the crystalline/crystalline polymer blends in order to obtain more and different novel superstructures.[32−36] However, most of the works focused on the crystallization behavior but ignored the phase morphologies. In addition, interplay between crystallization and phase separation in crystalline/crystalline polymer blends has seldom been studied so far.[37−41] Previously, we have investigated the effect of lower critical solution temperature (LCST) phase separation on the crystallization kinetics and morphology in the dynamically symmetric blend of poly(butylene succinate) (PBS)/poly(ethylene oxide) (PEO).[42] Because of the difficulties of mediating the dynamics of dual phase transitions, we found that there were many shortcomings in morphological controls. Furthermore, the pre-existing phase structures were easily destroyed by the subsequent crystal growth. In this work, the molecular weight of PEO is increased from M_n = 20 kg/mol to M_n = 1000 kg/mol. The large dynamic asymmetry comes from the wide molecular weight difference between slow PEO and fast PBS component. We are able to control the dynamics of the two phase transitions on a much wider time scale. A variety of novel pattern formations of PBS can be controlled and fixed by the slow phase of PEO. Furthermore, after a second quench to a temperature below the melting point of PEO, the final crystalline morphology and spatial distribution of both components can also be controlled effectively by the initial phase structures.

2. EXPERIMENT SECTION

2.1. Materials and Blend Sample Preparation. PEO with a number-average molecular weight of 1000 kg/mol was purchased from Sigma-Aldrich Company. PBS was provided by the Technical Institute of Physics and Chemistry (Chinese Academy of Sciences), with a relative number-average molecular weight of 86 kg/mol. The molecular weight was characterized by gel permeation chromatography (GPC) with eluent of chloroform and polystyrene as the standards. The glass transition temperatures of PBS and PEO were −30 and −60 °C, respectively. The blends were prepared by solution-casting using chloroform as a solvent, with a total weight fraction of 1%. The mixed polymer solutions were cast on the Petri dishes and dried in a vacuum oven until constant weight. The melting temperatures of PBS and PEO ($T_{m,PBS}$ and $T_{m,PEO}$) were measured to be about 114 and 64 °C, respectively.

2.2. Temperature Protocols. The PBS/PEO (75/25 w/w) blends were chosen for the viscoelastic phase separation and crystallization investigation. The blends were first heated to a selected VPS temperature of 180 °C and annealed for different times. After annealing, the demixed blends were quickly quenched to predetermined $T_{c,PBS}$ ($T_{m,PEO} < T_{c,PBS}$) for the crystallization of PBS. At last, the samples were further cooled to 40 °C for the crystallization of PEO.

2.3. Optical Microscopy. Phase contrast optical microscopy (PCOM) and polarized optical microscopy (POM) images were observed by an Olympus (BX51) optical microscope equipped with an Olympus camera (C-5050ZOOM). The samples were sandwiched in two glass plates and trapped by silicon oil to prevent degradation. The sample temperatures were controlled by a Linkam (LTS 350) hot stage. The area ratio of PEO-rich phase was obtained after processing the original images by digital image analysis software of ImageJ.

2.4. Differential Scanning Calorimeter. The isothermal diagrams were recorded by differential scanning calorimeter (DSC) (Q2000 TA Instruments) under a nitrogen atmosphere. The temperature and heat flow were calibrated by pure indium. The Avrami equation[43,44] was used to analyze the crystallization kinetics, as given in eqs 1 and 2

$$1 - X_c(t) = \exp(-kt^n) \quad (1)$$

$$\log[-\ln(1 - X_c(t))] = n \log t + \log k \quad (2)$$

where X_c is the weight fraction crystallinity, n is the Avrami index, and k is the overall rate constant.

2.5. Scanning Electron Microscopy. Samples were observed by a Hitachi S4300 scanning electron microscope (SEM) after being coated with platinum (Pt). Before SEM observation, all the blends were etched by ethanol to remove the crystals of PEO.

3. RESULTS AND DISCUSSION

3.1. Development of Structures in Viscoelastic Phase Separation. On the basis of our previous work, we have determined the LCST phase diagram of dynamically symmetric PBS/PEO blend and the critical point located above the melting temperature of PBS.[42] As the molecular weight of PEO increased from 20 to 1000 kg/mol, the components of PBS and PEO became immiscible in the accessible temperature range;

dx.doi.org/10.1021/ma5001496 | Macromolecules 2014, 47, 1741−1748

therefore, the phase diagram could not be quantitatively determined. Because of the large difference of relaxation time between both components ($\tau_{PEO}/\tau_{PBS} > 10^4$), PEO and PBS molecules showed different responses to the thermodynamic driving force, leading to the VPS process (see Supporting Information, Figure S1).

Figure 1 shows the PCOM images of PBS/PEO (75/25) blends at the VPS temperature of 180 °C for different annealing

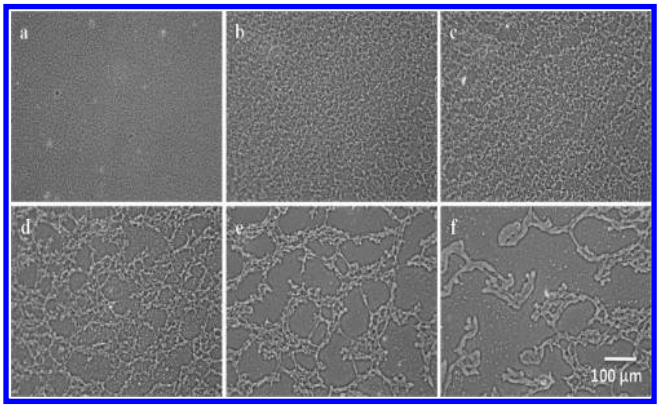

Figure 1. Phase contrast optical micrographs of the PBS/PEO (75/25 w/w) samples annealed at 180 °C for (a) 5, (b) 30, (c) 60, (d) 120, (e) 180, and (f) 360 min. The bright phase was PEO-rich phase.

times. The PBS/PEO blends were immiscible initially after solution blending. It was observed that the local concentration grew quickly and a network-like structure formed immediately (5 min of VPS time) as shown in Figure 1a. The network was formed by the interconnected bright PEO-rich phase, even though PEO was the minor component. With the increase of VPS time, the network began to merge and coarsen; meanwhile, the dark PBS-rich phase dispersed inside the matrix of PEO network (see Figure 1b,c). The long/thin strip structure could stay for a long time, which was significantly determined by the shear stress.[10] Here the effect of shear stress exceeded the influence of surface tension and maintained the interface stability of the network.[8] As the shear stress relaxed with time, the interface energy began to dominate the evolution of network-like structure. Then, the thin parts of the network were elongated and broken up randomly on a large scale (see Figure 1d,e). Among the large network, many small networks grew slowly on local scales and kept the shapes for a long time. It is noted that the network-like structures developed hierarchically on different length scales. The multilevel network-like pattern was dominated by the "elastic force balance" condition.[10−12,16] In the late stage of phase separation as shown in Figure 1f, the network-like structures relaxed to a rounded-shaped structure. This structure was dominated by the competition between interface tension and molecular relaxation. The dispersed PBS-rich domains turned into a usual majority matrix, which was a typical feature of phase inversion process during the viscoelastic phase separation (VPS). Accompanied by the phase inversion, the total volume of the PEO-rich domains kept decreasing, and the contrast of the two phases became more and more pronounced, which was known as the volume shrinking process.[8−10]

The area ratio of PEO-rich phase versus VPS time was plotted as shown in Figure 2a. At the beginning of the phase separation, the area percentage of PEO-rich phase was almost 65%, although the weight ratio of PEO was only 25%. It was

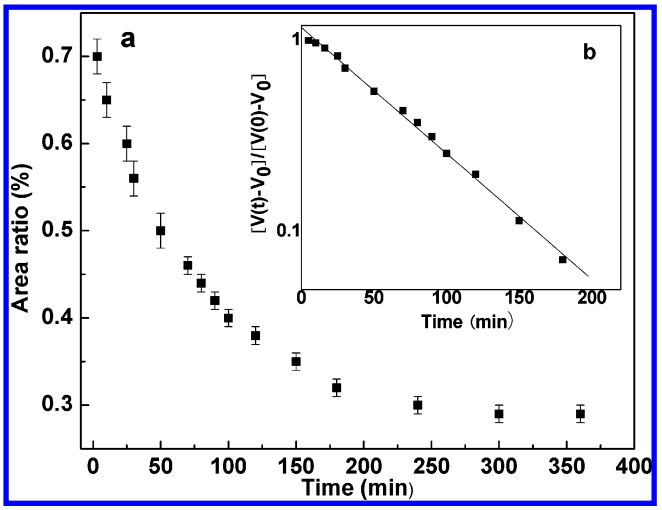

Figure 2. (a) Temporal changes in the area fraction of PEO-rich phase. (b) Volume fraction $((V(t) - V_0)/(V(0) - V_0))$ decreases exponentially with time.

implied that the content of PBS was extremely high within the interconnected PEO-rich domains. The volume decayed at a fast rate initially and then approached a constant value (30%) as VPS time reached beyond 180 min. Though the system was highly thermodynamically unstable at beginning, the PEO-rich phase of slower dynamics could not reach to the equilibrium state in a short time due to the slow mobility of PEO chains. Based on the viscoelastic model proposed by Tanaka,[8−10] the volume shrinking was resulted by the competition between driving force of concentration growth and the bulk stress. The VPS process could be divided into three regimes: diffusive regime, elastic regime, and hydrodynamic regime.[45] In the elastic growth region (about ≤180 min of VPS time), the volume fraction of PEO-rich phase decreased steeply with time; meanwhile, the minority PEO-rich phase reached toward the equilibrium state gradually. In the hydrodynamic growth region (about >180 min of VPS time), the volume fraction was almost constant as the two phases approached the equilibrium compositions.

According to the viscoelastic model by Tanaka,[45] the temporal evolution of structures obeyed a scaling law as shown in Figure 2b, and the volume fraction $((V(t) - V_0)/(V(0) - V_0))$ decreased exponentially with time, where $V(0)$ and V_0 were the initial and final area of PEO-rich phase.[16] The characteristic time τ of volume shrinking in this study could also be obtained with the relation $((V(t) - V_0)/(V(0) - V_0)) = \exp(-t/\tau)$. The value of τ was about 66 min. As stated above, the evolution of network-like structure, phase inversion, and volume shrinking were all determined by the competition between the thermodynamic instability and the slow dynamic mobility; meanwhile, the shear stress and bulk stress demonstrated their importance in these structural evolution processes.[8−10]

3.2. Crystallization of PBS Affected by the Pre-existing Phase Morphology during Double Quench Experiments. *3.2.1. Crystal Nucleation.* The hierarchical and various phase morphologies could be mediated in this phase separating crystalline/crystalline blend via VPS dynamics. In order to investigate the effect of VPS process on the crystallization, a series of double-quench experiments were carried out. The effect of VPS process on primary crystal nucleation process was studied. As shown in Figure 3, PBS

dx.doi.org/10.1021/ma5001496 | Macromolecules 2014, 47, 1741−1748

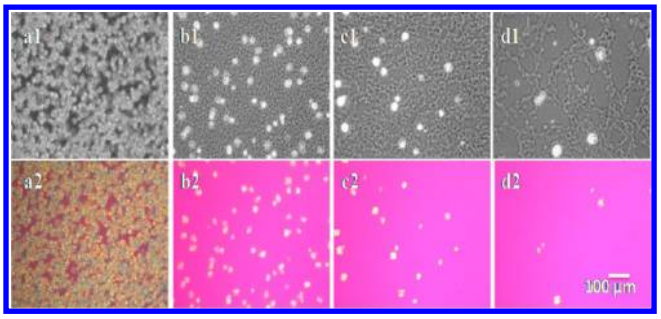

Figure 3. PCOM (upper row) and corresponding POM (lower row) patterns of the PBS/PEO (75/25 w/w) samples crystallized at 90 °C for 2 min after VPS at 180 °C for (a) 5, (b) 30, (c) 60, and (d) 180 min.

crystallized at 90 °C for 2 min, following the VPS processes at 180 °C for different times. It was observed that the nucleation density significantly decreased with the increase of VPS time. The nucleation density in Figure 3a (5 min of VPS time) was almost 20 times larger than that in Figure 3d (180 min of VPS time). As reviewed, the interface-assisted crystallization has been widely investigated in the dynamically symmetric polymer blends. The mechanism of "concentration fluctuation-assisted crystallization" was proposed by Han and co-workers.[24−27] It was described that the fluctuation could induce the chain segmental alignment to assist the crystallization. However, in the dynamically asymmetric polymer blends, due to the large effect of slow molecular relaxation, the contribution of concentration fluctuation was suppressed and could be neglected in this case.[8,10] On the contrary, the static heterogeneous nucleation at the interface became the main factor. As the transient network-like structure was elongated and eventually broken up with VPS time, the interfacial area of phase domains decreased sharply. When the crystallization temperature of PBS increased to 100 °C as shown in Figure 4,

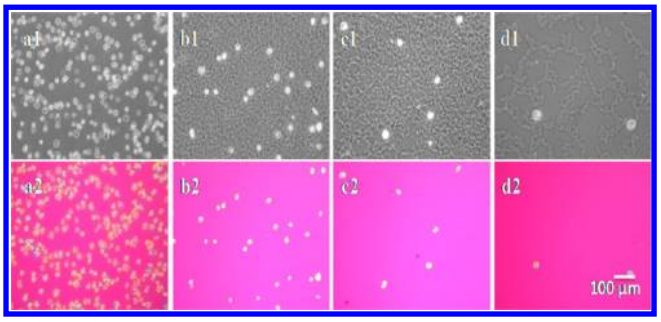

Figure 4. PCOM (upper row) and corresponding POM (lower row) patterns of the PBS/PEO (75/25 w/w) samples crystallized at 100 °C for 5 min after VPS at 180 °C for (a) 5, (b) 30, (c) 60, and (d) 180 min.

the same tendency of nucleation process was also observed. The longer VPS proceeded, the less nucleation density was observed. It was noted that the nucleation rate of PBS was determined by the total interfacial area between PBS and PEO phase domains (see Figures 3 and 4).

As stated above, it was observed that the nuclei were more inclined to form at the interface of phase domains. Though the interface-assisted crystallization was predicted and proved theoretically, it was still lack of some direct and convincing evidence on the macroscopic scale. To obtain a better understanding of the interface-assisted crystallization of PEO, some higher resolution microscopies have been also carried out. By comparing with the phase and crystallization morphologies, the location of nucleation could be checked clearly as shown in Figure 5. The PBS crystals formed (at 90 °C) at the interface of

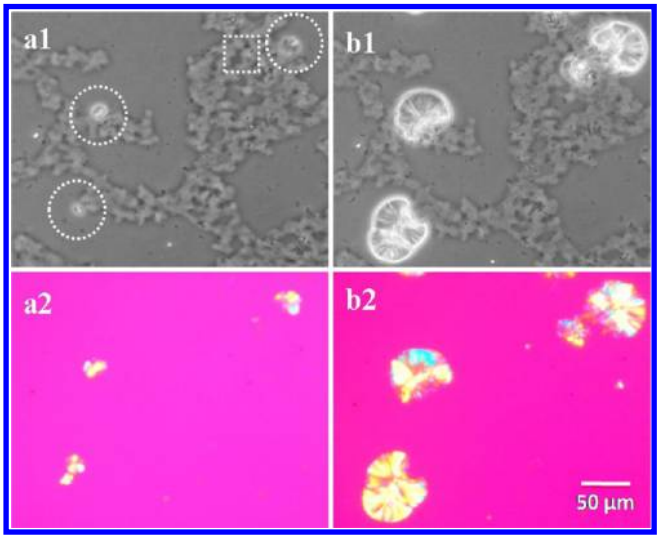

Figure 5. PCOM (upper row) and corresponding POM (lower row) patterns of the PBS/PEO (75/25 w/w) samples crystallized at 90 °C for (a) 5 and (b) 25 min after VPS at 180 °C for 360 min.

phase domains after the VPS process (at 180 °C for 360 min). Because of the hierarchical structures of the network, the crystals nucleated in multiple occurrences along the network structures. On one hand, several crystals formed at the interface between the network and large PBS-rich domains, which were indicated by white circles in Figure 5a. Because of the large confinement effect of the PEO network, the crystals of PBS grew toward the PBS-rich domains, leading to the irregular spherulites around the PBS-rich domains as shown in Figure 5b. It was implied that the pre-existed phase morphologies really had significant epitaxial effect on the subsequent crystallization of PBS. On the other hand, the PBS crystal could also nucleate inside the network on much smaller scales denoted by the white box as shown in Figure 5a. Furthermore, the growth of these crystals was limited to the inside of the network, forming frustrated crystals as shown in Figure 5b.

3.2.2. Overall Crystallization Kinetics. The isothermal crystallization kinetics of PBS under different effect of VPS process was determined by DSC. As shown in Figures 6a1 and 6b1, PBS crystallized at 90 and 100 °C, respectively, after VPS process at 180 °C for different times. The relative crystallinity changes of PBS against crystallization time were investigated as shown in Figures 6a2 and 6b2. The Avrami index n and crystallization constant k are also listed in Table 1. The values of Avrami index n ranged from 2 to 3, indicating a heterogeneous type of nucleation. The values decreased in the range of 2.8−2.1 as VPS time increased, implying that the nucleation process was sensitive to the decrease of interfacial area.

The crystallization half-time ($t_{1/2}$), defined as the time when the relative crystallinity reached at 50%, was an important measure of overall kinetics. It was interesting that the values of $t_{1/2}$ first increased and then decreased with the increase of VPS time. The overall crystallization kinetics obtained by DSC was statistical averaged for the whole sample, including both crystal

dx.doi.org/10.1021/ma5001496 | *Macromolecules* 2014, 47, 1741−1748

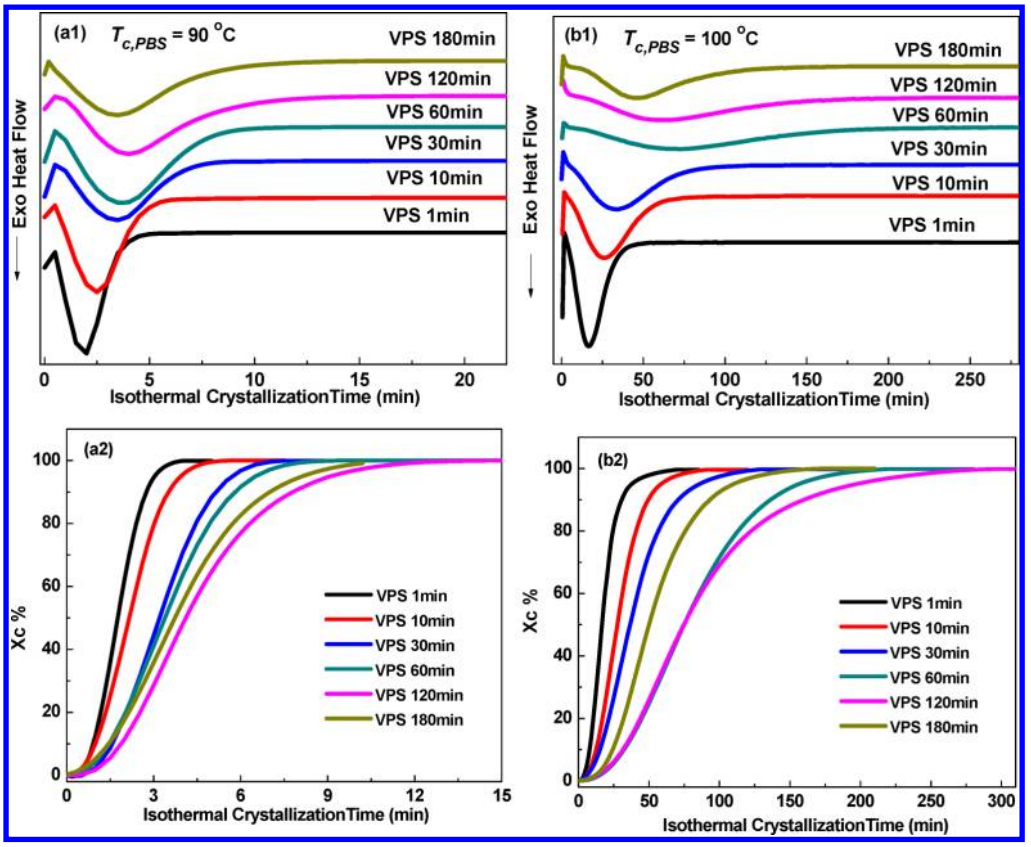

Figure 6. (1) DSC thermogram and (2) relative crystallinities of the PBS/PEO (75/25 w/w) samples obtained at (a) 90 °C and (b) 100 °C during isothermal crystallization after phase separation at 180 °C for different times.

Table 1. Avrami Parameters (n, k) and Half-Time of Crystallization ($t_{1/2}$)

	$T_{C,PBS}$ = 90 °C			$T_{C,PBS}$ = 100 °C		
VPS time (min)	n	$k \times 10^{-2}$ (min^{-n})	$t_{1/2}$ (min)	n	$k \times 10^{-4}$ (min^{-n})	$t_{1/2}$ (min)
1	2.8	14.3	1.7	2.6	5.0	16
10	2.4	10.2	2.1	2.5	1.9	27
30	2.3	7.0	3.3	2.5	1	37
60	2.3	3.9	3.4	2.3	0.3	75
120	2.3	3.1	4.2	2.3	0.3	75
180	2.1	5.0	3.7	2.2	0.9	51

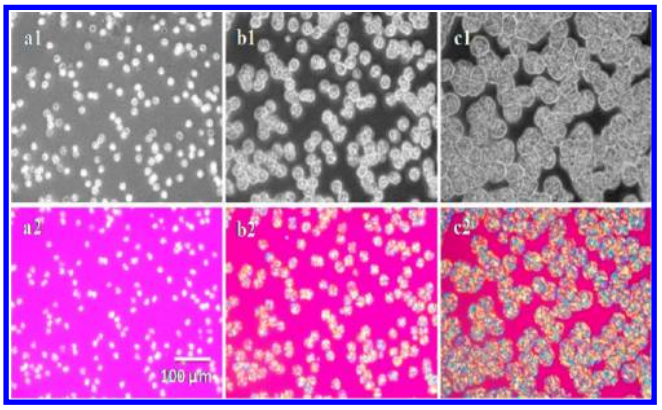

Figure 7. Time-resolved PCOM (upper row) and corresponding POM (lower row) patterns of the PBS/PEO (75/25 w/w) samples crystallized at 100 °C for (a) 5, (b) 10, and (c) 20 min after VPS at 180 °C for 5 min.

nucleation and growth rate. As stated above, the nucleation rate of PBS decreased significantly with the increase of VPS time. So the extraordinary kinetics must be caused by different mechanisms of crystal growth process. To better clarify the different effects on the crystals growth process of PBS due to the VPS, some time-resolved microscopy were also carried out.

3.2.3. Crystal Growth. Figure 7 shows the time-resolved PCOM and the corresponding POM patterns of PBS crystallized at 100 °C after annealing at 180 °C for 5 min. The typical compact PBS spherulites grew isotropically in the radial direction. The radius of PBS spherulites increased linearly with time, and the growth rate was estimated about 1.6 μm/min as shown in Figure S2. By comparing the phase and crystalline morphologies, the network-like structures were intercalated inside the spherulites of PBS. It is noted that the PBS crystals could penetrate the PEO network easily in the initial stage of VPS process.

As VPS time increased to 30 min, the PBS crystals nucleated somewhere within the coarsened network-like phase structures and then started to grow irregularly and broke through the network. The dendritic crystals were observed as shown in Figure 8. It is known that the crystal growth is dependent on two processes: the diffusion of the crystalline chains to and rearrange (secondary nucleation and growth) at the solid growth front and the repelling of amorphous chains out of the crystals.[18] As the crystals of PBS grew larger and larger, more PEO chains were excluded out of the crystals, and the noncrystallizing components were increasingly piled up at the front of crystal growth. The diffusion-controlled process came

dx.doi.org/10.1021/ma5001496 | Macromolecules 2014, 47, 1741−1748

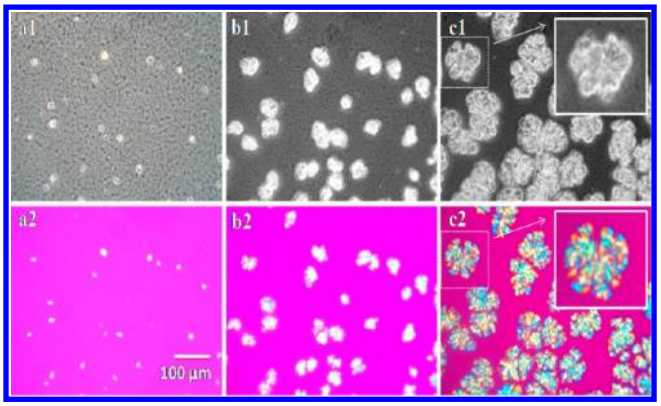

Figure 8. Time-resolved PCOM (upper row) and corresponding POM (lower row) patterns of the PBS/PEO (75/25 w/w) samples crystallized at 100 °C for (a) 10, (b) 30, and (c) 70 min after VPS at 180 °C for 30 min.

to dominate the crystal growth. The spherulite radius began to grow in a nonlinear fashion, and the growth rate became slower with crystallization time as shown in Figure S2.[20,21] Meanwhile, the slow relaxation of PEO molecules led to the internal stress, which caused the mechanical instability of the crystal growth front. As a result, the PBS spherulites grew irregularly and formed the dendritic crystals.

As VPS time increased to 180 min as shown in Figure 9, the network were elongated and broken up on a large scale, and the

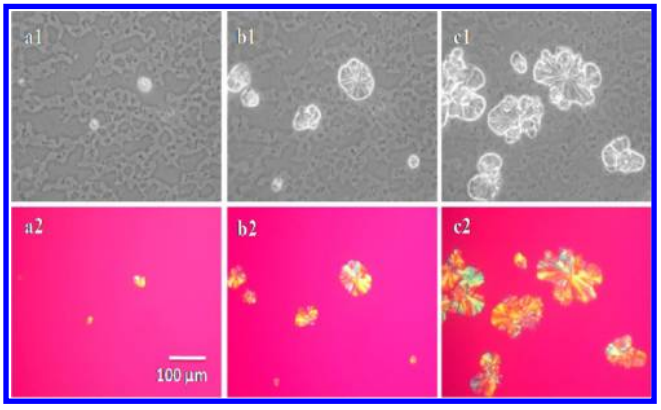

Figure 9. Time-resolved PCOM (upper row) and corresponding POM (lower row) patterns of the PBS/PEO (75/25 w/w) samples crystallized at 100 °C for (a) 10, (b) 20, and (c) 35 min after VPS at 180 °C for 180 min.

dark PBS-rich phases were dispersed randomly inside the network. The crystals started to nucleate at the boundary between phase domains or inside the isolated PBS-rich phase as shown in Figure 9a. The regular and compact spherulites grew isotropically within the PBS-rich domains at first as shown in Figure 9b, until the growth front encountered the network. Because of the large confinement effect of the network, the growth was limited and the crystals could not easily cross over the PEO-rich domains, leading to the irregular spherulites around the PBS-rich phase as shown in Figure 9c. The crystal structures were templated by the phase morphology. It was suggested that the pre-existing network had a significant epitaxial effect on the subsequent crystallization of PBS.

In our previous work, when the dynamically symmetric blends of PBS/PEO quenched to a certain crystallization temperature after annealing process, the liquid–liquid phase dissolution and crystallization took place simultaneously. The kinetics of phase dissolution was slower than the growth of crystallization.[42] However, in this case, due to the slow dynamics of molecular relaxation, the phase dissolution rate became much slower. Therefore, the effect of phase dissolution during the crystallization process could be neglected, and the growth of PBS was just influenced by the initial phase morphologies upon various VPS processes. The crystal growth rates of PBS via different VPS times are shown in Figure 10.

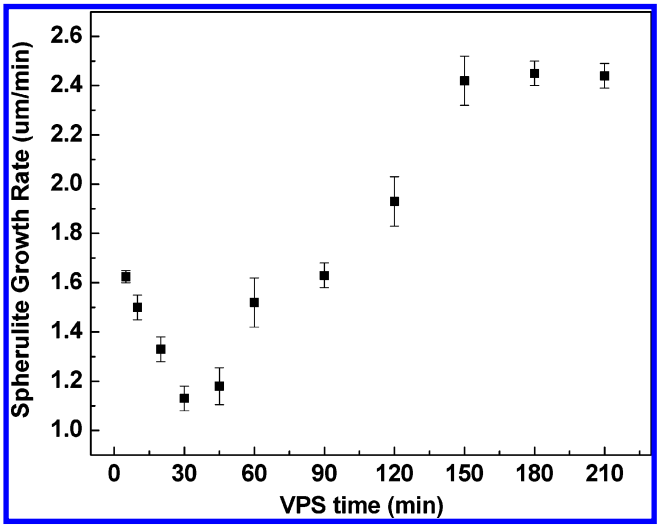

Figure 10. VPS time dependence of PBS spherulites growth rates.

With the increase of VPS time, the spherulite growth rate of PBS (G_{PBS}) first decreased slightly and reached the minimum at about 30 min of VPS time and then turned to increase sharply until reached 180 min of VPS time. As the VPS time further increased above 180 min, the growth rate remained constant (see Figure 10).

At the beginning of VPS process, the area percentage of the PEO network was about 65% (see Figure 2), implying that the content of PBS was extremely high within the PEO-rich phase domains. So the crystals of PBS could penetrate through the PEO network easily, and the spherulites grew linearly (see Figure S2). As VPS time increased to 30 min, the network began to shrink; meanwhile, the apparent volume percentage of PEO-rich phase decreased sharply. The PBS content of the PEO-rich phase was decreased substantially with time. So the diffusion of PBS molecules was restricted, and the crystal growth became more and more limited. As VPS time further increased to 180 min, the network was shrunk and broken up randomly, and the dispersed PBS-rich domains turned into the usual majority matrix. The crystals of PBS could grow inside the large and extended PBS-rich domains as shown in Figure 9. As a result, the growth rate of PBS began to increase toward the unconfined limit again. When VPS time was above 180 min, the growth rate remained constant because the two phases approached to the equilibrium compositions.

3.2.4. Effect of VPS on the Final Morphology. The mechanical properties of polymer blends are always related to the final phase morphology after phase separation and crystallization processes. For the crystalline/crystalline blend systems, the final morphology was determined by the interplay between crystallizations of both crystalline components. The VPS process allowed a wide range of compositional control in

dx.doi.org/10.1021/ma5001496 | *Macromolecules* 2014, 47, 1741–1748

the blends and consequently could provide a variety of novel phase structures.[13−16]

As shown in Figure 11, the SEM analysis was carried out to investigate the final crystalline morphology of PBS/PEO blends

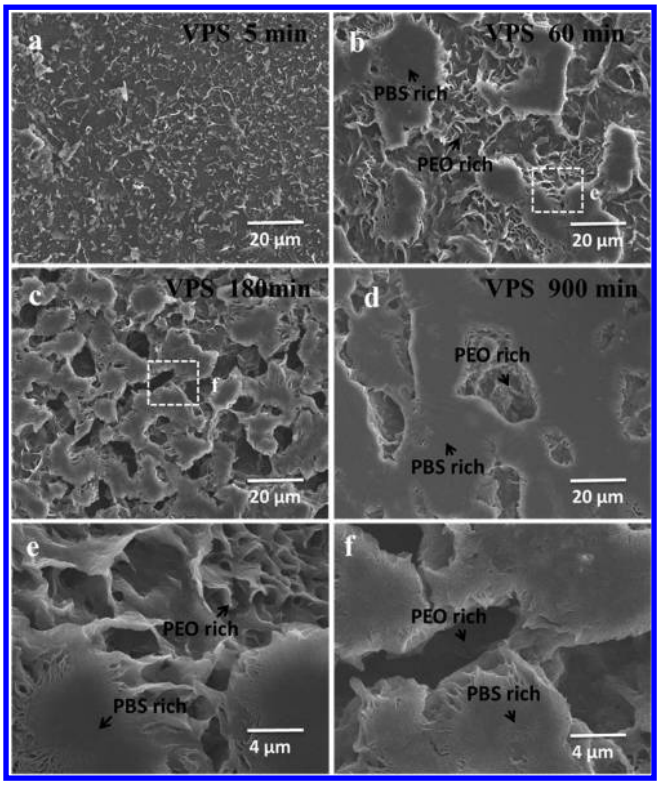

Figure 11. SEM images of the PBS/PEO (75/25 w/w) samples crystallized at 80 °C for 120 min after VPS at 180 °C for (a) 5, (b) 60, (c) 180, and (d) 900 min and then crystallized subsequently at 40 °C for 60 min. PEO was etched by alcohol before observation. Images e and f were enlarged of the square box in images b and c.

after VPS at 180 °C for different times. PBS crystallized at 80 °C for 120 min, and then PEO crystallized at 40 °C for 60 min subsequently. The PEO crystals were etched by alcohol for 3 days before observation. When VPS time was 5 min, the network-like structures of PEO could be observed as shown in Figure 11a. As stated above, the content of PBS was extremely high within the PEO-rich phase domains at the beginning of VPS, so the PEO-rich phase domains were unable to be etched completely. Consequently, the area ratio of etched network-like structures did not exactly correspond to the PCOM results. As VPS time increased to 60 min, the phase structure coarsened and the PBS-rich phase dispersed as isolated domains inside the matrix of PEO network, as shown in Figure 11b. Figure 11e shows the detailed crystalline structures within the PEO-rich and PBS-rich phase domains. The interconnected cellular-like structure was observed in the etched PEO-rich domains. On the contrary, the crystalline structure in the PBS-rich domains was compact. With the further increase of VPS time, the phase structure grew and coarsened; meanwhile, the isolated PBS-rich domains turned into the continuous phase structure. Because of the epitaxial effect of pre-existing phase morphology, the crystallization structures of PBS were also continuous and interconnected as shown in Figure 11c. As stated above, the volume fraction of the two phases was very close to the equilibrium state when VPS time increased to 180 min. Thus, the PBS crystals could hardly penetrate the PEO-rich domains. Furthermore, the crystals of PEO had been etched completely and left big cavities as shown in Figure 11f. As VPS time increased to 900 min, the PBS-rich domains turned into a usual majority matrix accompanied by the phase inversion. By contrast, the crystals of PEO dispersed within the matrix of PBS as shown in Figure 11d.

4. CONCLUSIONS

In this work, we have investigated the VPS process in the dynamically asymmetric crystalline/crystalline polymer blends of PBS/PEO. The hierarchical network was formed by the slow dynamics of PEO-rich phase, even though PEO was the minor component. The evolution of network-like structures, phase inversion, and volume shrinking were studied by PCOM, which were determined by the competition between large thermodynamic instability and slow dynamic mobility.

The interplay between crystallization and VPS process was also studied. In conclusion, the crystal nucleation and growth were significantly influenced by the initial phase morphology. According to the effect of interface-assisted crystallization, the nuclei of PBS were more inclined to form at the interface of phase domains. The nucleation density decreased with the decrease of interfacial area. Meanwhile, the corresponding crystal growth rate was also dependent on the VPS process. After 5 min of annealing at 180 °C, the content of PBS was extremely high within the interconnected PEO-rich phase; therefore, the crystals of PBS could penetrate through the PEO network easily. As the network-like structures coarsened, the PBS content of the PEO-rich phase was decreased substantially with time. So the diffusion of PBS molecules was restricted, and the crystal growth became more and more confined. As VPS time further increased to 180 min, the network was elongated and broken up randomly, and the dispersed PBS-rich domains turned into a usual majority and continuous matrix. The crystals of PBS grew inside the PBS-rich domains without restrictions, and the growth rate of PBS began to increase sharply. When VPS time was above 180 min, compositions of the two phases approached to the equilibrium state, and the growth rate began to remain constant.

The final crystalline morphology and spatial distribution of both components were also significantly controlled by the initial phase morphology. As the minor phase of PEO going through the inversion from transient network to dispersed domains, the final mechanical and other possible functional properties could be controlled between the properties of neat PBS and PEO. Compared to dynamically symmetric polymer systems, the VPS process provided more possibilities to design the final phase and crystallization morphologies conveniently in such immiscible crystalline/crystalline polymer blends.

■ ASSOCIATED CONTENT

Supporting Information

Figures S1 and S2. This material is available free of charge via the Internet at http://pubs.acs.org.

■ AUTHOR INFORMATION

Corresponding Authors

*E-mail c.c.han@iccas.ac.cn; Tel +86 10 82618089; Fax +86 10 62521519 (C.C.H.).

*E-mail liangyr@iccas.ac.cn; Tel +86 10 82618089; Fax +86 10 62521519 (Y.L.).

Notes

The authors declare no competing financial interest.

■ ACKNOWLEDGMENTS

This research work was supported by National Natural Science Foundation of China (No. 50930003, No. 21004070, and No. 21374125).

■ REFERENCES

(1) Paul, D. R.; Newman, S. *Polymer Blends*; Academic Press: New York, 1978.
(2) Cheng, S. Z. D. *Phase Transitions in Polymers: the Role of Metastable States*; Elsevier: Boston, MA, 2008.
(3) Li, J. Y.; Li, W.; Li, Z. Y.; Cheng, H.; Li, Y.; Han, C. C. *J. Chem. Phys.* **2011**, *135*, 4902.
(4) Pincus, P. *J. Chem. Phys.* **1981**, *75*, 1996−2000.
(5) Binder, K. *J. Chem. Phys.* **1983**, *79*, 6387−6409.
(6) De Gennes, P. G. *J. Chem. Phys.* **1980**, *72*, 4756.
(7) Hashimoto, T.; Kumaki, J.; Kawai, H. *Macromolecules* **1983**, *16*, 641−648.
(8) Tanaka, H. *Macromolecules* **1992**, *25*, 6377−6380.
(9) Tanaka, H. *Phys. Rev. E* **1997**, *56*, 4451−4462.
(10) Tanaka, H. *J. Phys.: Condens. Matter* **2000**, *12*, 207−264.
(11) Tanaka, H.; Araki, T. *Phys. Rev. Lett.* **1997**, *78*, 4966−4969.
(12) Tanaka, H. *Adv. Mater.* **2009**, *21*, 1872−1880.
(13) Shi, W. C.; Cheng, H.; Chen, F. H.; Liang, Y. R.; Xie, X. M.; Han, C. C. *Macromol. Rapid Commun.* **2011**, *32*, 1886−1890.
(14) Koyama, T.; Araki, T.; Tanaka, H. *Phys. Rev. Lett.* **2009**, *102*, 5701.
(15) Zhang, Y.; Shi, W. C.; Chen, F. H.; Han, C. C. *Macromolecules* **2011**, *44*, 7465−7472.
(16) Shi, W. C.; Chen, F. H.; Zhang, Y.; Han, C. C. *ACS Macro Lett.* **2012**, *1*, 1086−1089.
(17) Cheng, S. Z. D.; Keller, A. *Annu. Rev. Mater. Sci.* **1998**, *28*, 533−562.
(18) Muthukumar, M. *Adv. Chem. Phys.* **2004**, *128*, 1−63.
(19) Lotz, B. *Macromolecules* **2012**, *45*, 2175−2189.
(20) Tanaka, H.; Nishi, T. *Phys. Rev. Lett.* **1985**, *55*, 1102−1105.
(21) Tanaka, H.; Nishi, T. *Phys. Rev. A* **1989**, *39*, 783−794.
(22) Wang, H.; Shimizu, K.; Kim, H.; Hobbie, E. K.; Wang, Z. G.; Han, C. C. *J. Chem. Phys.* **2002**, *116*, 7311−7315.
(23) Shimizu, K.; Wang, H.; Wang, Z. G.; Matsuba, G.; Kim, H.; Han, C. C. *Polymer* **2004**, *45*, 7061−7069.
(24) Zhang, X. H.; Wang, Z. G.; Muthukumar, M.; Han, C. C. *Macromol. Rapid Commun.* **2005**, *26*, 1285−1288.
(25) Zhang, X. H.; Wang, Z. G.; Dong, X.; Wang, D. J.; Han, C. C. *J. Chem. Phys.* **2006**, *125*, 4907.
(26) Zhang, X. H.; Wang, Z. G.; Zhang, R. Y.; Han, C. C. *Macromolecules* **2006**, *39*, 9285−9290.
(27) Du, J.; Niu, H.; Dong, J. Y.; Dong, X.; Wang, D.; He, A.; Han, C. C. *Macromolecules* **2008**, *41*, 1421−1429.
(28) Mitra, M. K.; Muthukumar, M. *J. Chem. Phys.* **2010**, *132*, 4908.
(29) Shi, W. C.; Xie, X. M.; Han, C. C. *Macromolecules* **2012**, *45*, 8336−8346.
(30) Shi, W. C.; Han, C. C. *Macromolecules* **2012**, *45*, 336−346.
(31) Shi, W. C.; Yang, J.; Zhang, Y.; Luo, J.; Liang, Y. R.; Han, C. C. *Macromolecules* **2012**, *45*, 941−950.
(32) He, Y.; Zhu, B.; Kai, W. H.; Inoue, Y. *Macromolecules* **2004**, *37*, 3337−3345.
(33) Ikehara, T.; Kimura, H.; Qiu, Z. B. *Macromolecules* **2005**, *38*, 5104−5108.
(34) Liu, J. P.; Jungnickel, B. J. *J. Polym. Sci., Part B: Polym. Phys.* **2007**, *45*, 1917−1931.
(35) Qiu, Z. B.; Yan, C. Z.; Lu, J. M.; Yang, W. T. *Macromolecules* **2007**, *40*, 5047−5053.
(36) Wang, T. C.; Li, H. H.; Wang, F.; Yan, S. K.; Schultz, J. M. *J. Phys. Chem. B* **2011**, *115*, 7814−7822.
(37) Fujita, K.; Kyu, T.; Manley, R. S. J. *Macromolecules* **1996**, *29*, 91−96.
(38) Chuang, W. T.; Jeng, U. S.; Sheu, H. S.; Hong, P. D. *Macromol. Res.* **2006**, *14*, 45−51.
(39) Chuang, W. T.; Jeng, U. S.; Hong, P. D.; Sheu, H. S.; Lai, Y. H.; Shih, K. S. *Polymer* **2007**, *48*, 2919−2927.
(40) Nurkhamidah, S.; Woo, E. M. *J. Phys. Chem. B* **2011**, *115*, 13127.
(41) Nurkhamidah, S.; Woo, E. M. *Macromolecules* **2012**, *45*, 3094−3103.
(42) He, Z. Y.; Liang, Y. R.; Wang, P. L.; Han, C. C. *Polymer* **2013**, *54*, 2355−2363.
(43) Vilanova, P.; Ribas, S. *Polymer* **1985**, *26*, 423−428.
(44) Raka, L.; Sorrentino, A.; Bogoeva-Gaceva, G. *J. Polym. Sci., Part B: Polym. Phys.* **2010**, *48*, 1927−1938.
(45) Tanaka, H. *Phys. Rev. Lett.* **1996**, *76*, 787−790.